Thermochemical evolution of the sub-arc mantle due to back-arc spreading

Paul S. Hall,[1] Lauren B. Cooper,[2] and Terry Plank[3]

Received 3 May 2011; revised 29 November 2011; accepted 1 December 2011; published 1 February 2012.

[1] We present the results of a series of numerical geodynamic experiments designed to characterize the thermal and compositional evolution of the sub-arc mantle in response to spreading in the back-arc. We find large changes in both the temperature and composition of the sub-arc mantle with time as the BASC migrates away from the arc. In particular, the sub-arc mantle becomes increasingly more depleted with time following the onset of spreading, as mantle that has experienced decompression melting and melt extraction beneath the BASC is gradually drawn beneath the arc plate by slab-induced corner flow. The rate at which this depletion increases during the ~2 Myr immediately following the onset of spreading is controlled by the spreading rate at the BASC, with faster spreading leading to a more rapid increase in depletion. Following this initial period, depletion within the sub-arc mantle continues to increase at a somewhat slower pace. During this phase, the rate at which depletion increases is chiefly dictated by the subduction rate, with faster subduction leading to a more rapid increase in depletion beneath the arc. Depletion within the sub-arc mantle is also found to increase with increasing mantle potential temperature, decreasing age of the overriding plate, and decreasing distance between the initial location of the BASC and the arc. Predicted changes in the depletion of the sub-arc mantle with time are shown to be consistent with observations of systematic along-strike geochemical variations within a portion of the Tonga Arc adjacent to the Eastern Lau Spreading Center.

Citation: Hall, P. S., L. B. Cooper, and T. Plank (2012), Thermochemical evolution of the sub-arc mantle due to back-arc spreading, *J. Geophys. Res.*, *117*, B02201, doi:10.1029/2011JB008507.

1. Introduction

[2] Back-arc basins are complex tectonic environments where hydrous melting processes associated with island arc volcanism may be juxtaposed with decompression melting processes at back-arc spreading centers (BASCs). The interaction between these two distinct melting processes results in strong gradients in both geochemical and geophysical observables within the back-arc basin, providing an important window on geodynamic and petrogenetic processes at both divergent and convergent plate boundaries [*Martinez and Taylor*, 2002; *Taylor and Martinez*, 2003; *Kelly et al.*, 2006; *Langmuir et al.*, 2006; *Wiens et al.*, 2006; *Dunn and Martinez*, 2011]. The depletion of high field strength elements (HFSEs) relative to large ion lithophile elements (LILEs) in island arc lavas within arc-BASC systems may be one consequence of such interactions. In particular, several studies have suggested that this depletion is due to melting at the BASC, which creates a residual mantle that is depleted in highly incompatible elements, including LILEs and HFSEs. This depleted residue is then advected beneath the adjacent arc where it is fluxed with a fluid released from subducting plate that is rich in LILEs but poor in fluid immobile HFSEs. This leads to flux melting of the residue, generating magma that is depleted in HFSEs relative to LILEs and is erupted at the arc [*McCulloch and Gamble*, 1991; *Woodhead et al.*, 1993; *Caulfield et al.*, 2008]. The feasibility of this so-called pre-conditioning model of the relative depletion of HFSEs in arc magmas has been demonstrated using numerical geodynamic models [*Kincaid and Hall*, 2003].

[3] The recent discovery of high-Ca boninites at an active submarine volcano in the Tonga Arc, along with petrological evidence for a compositional gradient in parental magmas along the Tonga Arc, have led to a refinement of the pre-conditioning model in which depletion of the sub-arc mantle varies with time [*Cooper et al.*, 2010]. Specifically, the formation of boninitic parental magmas at the Tonga Arc requires that the mantle source experiences high cumulative degrees of partial melting (>24%). *Cooper et al.* [2010] suggest that this is accomplished through a multistage melting model similar to the pre-conditioning model. In particular, prior to extension in the back-arc, fertile peridotite is advected beneath the arc by slab-induced corner flow

[1]Department of Earth Sciences, Boston University, Boston, Massachusetts, USA.
[2]Department of Mineralogy, University of Geneva, Geneva, Switzerland.
[3]Lamont-Doherty Earth Observatory, Earth Institute at Columbia University, Palisades, New York, USA.

0148-0227/12/2011JB008507

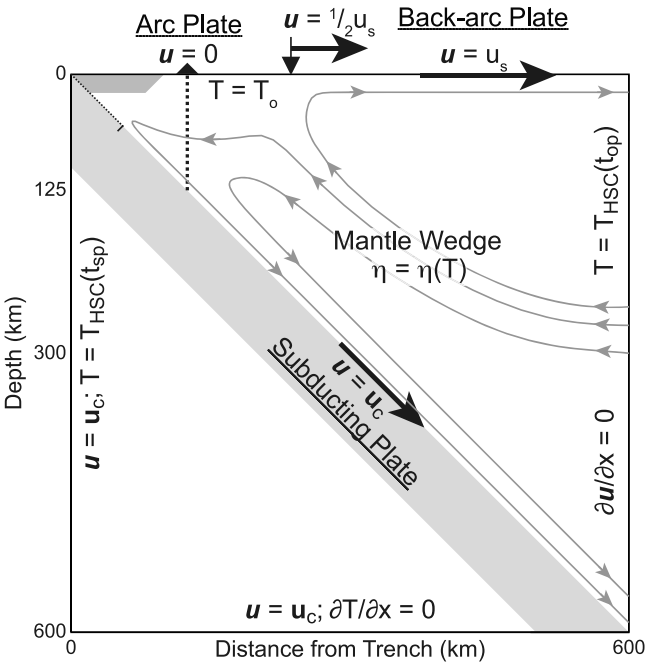

Figure 1. Schematic representation of the model geometry and boundary conditions, and resulting flow in the mantle wedge. The nominal location of the arc is indicated by a small, black triangle with a vertical dotted line extending beneath to indicate the location of sub-arc profiles shown in later figures. The location of the back-arc spreading center, which migrates away from the trench at half the spreading rate, is shown by the inverted black triangle. The dark gray portion of the arc plate is treated as rigid. The mantle wedge is only partially coupled to the subducting plate at depths less than 70 km, as indicated by the dotted line along the surface of the subducting plate. A full list of parameter names and values is given in Table 1.

where it is fluxed by fluids expelled from the downgoing slab, generating a melt with relatively high Ti_6 and low Si_6 (concentrations of TiO_2 and SiO_2 at 6 wt% MgO) that is erupted at the arc. With the onset of spreading in the back-arc, the fertile peridotite experiences an initial phase of melting due to decompression beneath the BASC. This depletes the peridotite of incompatible elements prior to its being advected beneath the arc to undergo flux melting, resulting in a magma that has lower Ti_6 and higher Si_6 than would be produced from an undepleted source. Systematic variations in Ti_6 and Si_6 along the strike of the Tonga arc indicate that parental arc magmas range from boninitic (highly depleted source) to incompatible element depleted basalt (depleted source) to typical arc basalt (little to no depletion of the source). Spatially, the most depleted sources correspond to the portions of the arc at which spreading in the back-arc has been occurring longest, while the least depleted sources occur in regions where back-arc spreading began only recently [*Cooper et al.*, 2010], implying a time-dependence to the depletion of the sub-arc mantle. Based on simple geometric arguments, *Cooper et al.* [2010] suggest that following the onset of spreading, residual mantle from the base of the melting column beneath the BASC, which has experienced only small degrees of melting and melt extraction, is advected beneath the arc before mantle from further up in the melting column, which has experienced greater degrees of melting, follows. This results in a gradual increase in the depletion of the sub-arc mantle.

[4] The present work focuses on testing the conceptual model of the evolution of the sub-arc mantle following the onset of spreading in the back-arc of *Cooper et al.* [2010] using a numerical geodynamic model. The approach taken differs from previous geodynamic modeling of mantle flow and melting in arc-BASC systems [*Toksoz and Hsui*, 1978; *Kincaid and Hall*, 2003; *Currie et al.*, 2004; *Conder*, 2005; *Currie and Hyndman*, 2006; *Harmon and Blackman*, 2010] in that the time-dependent nature of the system is considered explicitly. In particular, the migration of the BASC away from the trench as a natural consequence of spreading [*Ribe*, 1989; *Lin et al.*, 2010] is incorporated directly into the model. We find large changes in both the temperature and the composition of the sub-arc mantle with time, as the BASC migrates away from the arc, that are consistent with the evolutionary model of *Cooper et al.* [2010].

2. Methods

[5] Mantle flow and melting within arc-BASC systems is modeled assuming an idealized, 2-dimensional geometry and adopting a frame of reference fixed to the trench. In particular, the subducting plate sinks through the model domain at a constant angle of 45° (Figure 1). While geodynamic models of individual subduction zones and arc-BASC systems benefit from the use of more realistic, seismically constrained subducting plate geometries [*Harmon and Blackman*, 2010; *Lin et al.*, 2010; *Syracuse et al.*, 2010], the simplified geometry employed here is appropriate for a generic arc-BASC system. Likewise, the use of a 2-dimensional model precludes consideration of the complex flow patterns that may develop in 3-dimensional models due to, for example, slab rollback or along-strike variations in slab geometry or forcing [*Kincaid and Griffiths*, 2003; *Schellart*, 2004; *Schellart et al.*, 2007; *Schellart*, 2008; *Jadamec and Billen*, 2010], but is suitable for the scope of the present study.

2.1. Governing Equations

[6] Flow within the mantle wedge is assumed to be driven purely kinematically through viscous coupling to the subducting plate and the overriding arc and back-arc plates (Figure 1). Buoyancy forces that might arise within the wedge are ignored, precluding a variety of convective instabilities [*Hall and Kincaid*, 2001; *Honda and Saito*, 2003; *Behn et al.*, 2007] that could introduce additional temporal- and spatial-variability to the flow. A small (20 km × 100 km)portion of the overriding arc plate immediately adjacent to subducting slab is treated as rigid to prevent excessive thinning of the cold boundary layer through viscous coupling to the subducting slab [*Conder*, 2005; *van Keken et al.*, 2008].

[7] Velocity within the mantle wedge is obtained from equations describing the conservation of mass and momentum for a viscous fluid with an infinite Prandtl number:

$$\nabla \cdot \mathbf{u} = 0 \tag{1}$$

$$\nabla \cdot \tau - \nabla p = 0, \tag{2}$$

Table 1. List of Parameters Along With Their Reference Value or Dimensions as Employed in the Numerical Experiments

Parameter	Symbol	Value	Dimensions
	Constants		
Activation energy	E	335	kJ mol^{-1}
Adiabatic gradient	ΔT_{adb}	0.3	°C km^{-1}
Age, subducting plate	t_{sp}	100	Myr
Density	ρ	3300	kg m^{-3}
Dynamic viscosity, maximum	$\eta_{\max}$	10^{26}	Pa s
Entropy of fusion	ΔS	400	J kg^{-1} °C^{-1}
Gas constant	R	8.314472	J °C^{-1} mol^{-1}
Heat capacity	C_p	1250	J °C^{-1} mol^{-1}
Mantle water content	C_{H_2O}	0.1	wt%
Potential temperature, surface	T_o	0	°C
Pre-exponential constant	A	1.32043×10^9	Pa s
Thermal conductivity	k	3	W m^{-1} °C^{-1}
	Experimental Parameters		
Age, overriding plate	t_{op}	25, 50, 75	Myr
Subduction rate	u_c	50, 100, 150, 200	km Myr^{-1}
Distance, arc-BASC	Δx_o	10, 25, 50, 75	km
Potential temperature, mantle	T_m	1300, 1350, 1400, 1450	°C
Spreading rate	u_s	25, 50, 75, 100	km Myr^{-1}
	Variables		
Depth	z	-	m
Deviatoric stress	τ	-	Pa
Dynamic pressure	p	-	Pa
Dynamic viscosity, diffusion creep	η_{diff}	-	Pa s
Dynamic viscosity, effective	η	-	Pa s
Latent heat loss	Φ_L	-	°C s^{-1}
Strain rate	$\dot{\epsilon}$	-	s^{-1}
Temperature	T	-	°C
Time	t	-	s
Velocity	$\mathbf{u}$	-	m s^{-1}

where $\mathbf{u}$ is velocity, p is dynamic pressure and τ is the deviatoric stress tensor. Deviatoric stress is related to velocity by

$$\tau = 2\eta\dot{\epsilon} = \eta\left(\nabla\mathbf{u} + (\nabla\mathbf{u})^{\mathrm{T}}\right), \tag{3}$$

where η is the effective dynamic viscosity and $\dot{\epsilon}$ is the strain rate tensor. We adopt a simplified, temperature-dependent diffusion creep rheology that ignores dependence on pressure, grain size, and water content [e.g., *van Keken et al.*, 2008]. The resulting viscosity is given by

$$\eta_{\mathrm{diff}}(T) = A\exp\left(\frac{E}{RT}\right). \tag{4}$$

The effective viscosity, η, is taken to be the minimum of η_{diff} and a maximum viscosity, $\eta_{\max}$, which is employed for computational expediency.

[8] Temperature (T) within the model domain is obtained from the equation describing the conservation of energy for a medium with constant density (ρ), heat capacity (C_p) and thermal conductivity (k), including a source term to account for latent heat associated with melting (Φ_L):

$$\frac{\partial T}{\partial t} = -\rho C_p(\mathbf{u}\cdot\nabla)T + \nabla\cdot(k\nabla T) - \Phi_L. \tag{5}$$

A complete list of variables and parameter values is given in Table 1. The model domain is discretized with an unstructured mesh of 13,984 triangular elements and the governing equations are solved subject to the relevant boundary conditions using the COMSOL Multiphysics finite element modeling package. The accuracy of the numerical model was tested by direct comparison to the subduction benchmark of *van Keken et al.* [2008].

[9] Melting is modeled using a Lagrangian particle method [*Hall and Kincaid*, 2003; *Kincaid and Hall*, 2003]. This particle-based approach allows the composition of discrete portions of the mantle to be tracked explicitly. This is of particular importance in arc-BASC systems, where flow varies with time as a result of the migration of the BASC, resulting in complex melting histories for individual parcels of mantle. A total of 100,000 particles are utilized to model melting within the mantle wedge in these experiments. The position of each individual particle is calculated at every timestep based on its previous position and the local velocity field, $\mathbf{u}$, using a 4th-order Runge-Kutta scheme. Melting is calculated using the hydrous melting parameterization of *Katz et al.* [2003]. This method, which takes a cryoscopic approach to the effect of water on melting, is conceptually similar to, but computationally simpler than, more recent parameterizations that also take into account varying solidi, pressure and partition coefficients [*Langmuir et al.*, 2006; *Hirschmann et al.*, 2009; *Kelley et al.*, 2010]. All of these cryoscopic parameterizations are simpler to implement than fully thermodynamic parameterizations [*Hebert et al.*, 2009]. Although the hydrous melting model employed here is simplified, it suits our goal of understanding how different tectonic drivers of flow beneath the back-arc affect the compositional evolution of the arc source. Future efforts to

predict specific melt volumes and compositions at individual arcs will require the use of more accurate, but more complex, parameterizations. Incremental melt production is calculated for each particle at every timestep, based on temperature, pressure and water content at its location, and the melting history of the particle prior to that time. The melt history of a particle is characterized by its depletion, which is to say the accumulated degree of melting and melt extraction it has experienced. We assume that any melt produced during a given timestep is extracted vertically to the surface (i.e., fractional melting), so the possibility of refertilization of the depleted residue by solidification of small degrees of melt within the mantle is not considered. Therefore, in practice, a particle's depletion is simply the sum of all of the incremental degrees of melting experienced by that particle up to that time, expressed as a weight fraction. For example, a particle that melted incrementally by 1% ($\Delta F = 0.01$) over each of four consecutive model time steps would have had 4% of its original mass removed and hence would have a depletion of 0.04. The change in temperature due to latent heat loss with the production of an incremental melt is calculated for that particle and the temperature field adjusted accordingly by averaging of the latent heat lost by each particle onto the nodes of the computational grid [*Hall and Kincaid*, 2003].

[10] For simplicity, we choose not to model the hydrous flux melting processes thought to play a dominant role in magma genesis at the arc and instead focus on adiabatic decompression melting of hydrous peridotite within the mantle wedge. This is consistent with our stated goal of understanding how melting beneath the BASC affects the characteristics of the mantle beneath arcs, as the presumed region of hydrous fluid addition is effectively downstream of both the arc and the BASC. However, it has been suggested that flux melting might contribute to melting beneath BASCs, particularly early in the evolution of arc-BASC systems, when the BASC is closest to the arc [*Martinez and Taylor*, 2002; *Taylor and Martinez*, 2003; *Kelly et al.*, 2006; *Langmuir et al.*, 2006; *Harmon and Blackman*, 2010; *Lin et al.*, 2010]. To model the effect of water on decompression melting beneath a BASC we employ a uniform water content throughout the entire mantle wedge. The distribution of water within the mantle wedge is likely to be complex, with concentrations increasing from the back-arc to the arc [*Kelly et al.*, 2006]. However, there are large uncertainties in the spatial and temporal distribution of water in the mantle wedge above subducting slabs related to the mechanisms of fluid transport [*Cagniocle et al.*, 2007; *Hebert et al.*, 2009]. We adopt a water content of 0.1 wt%, which is well within the bounds of observed mantle water contents at BASCs, but significantly lower than values inferred beneath arcs [*Kelly et al.*, 2006].

2.2. Boundary Conditions

[11] Boundary conditions used in solving the governing equations are illustrated in Figure 1. Along the left and bottom boundaries velocity is set to that of the subducting plate (u_c), while the right hand boundary is stress free. Along the top boundary, velocity is prescribed in two distinct zones. In the area corresponding to the arc plate, the boundary is treated as fixed ($\mathbf{u} = \mathbf{0}$). In the area of the back-arc plate, velocity is fixed to the full spreading rate of the BASC ($\mathbf{u} = \mathbf{u_s}$). The point of contact between the arc and back-arc plates, where the divergence in velocity induces upwelling within the mantle, is the BASC. The location of this contact point is allowed to evolve with time, moving to the right at a velocity equal to the half-spreading rate at the BASC ($\mathbf{u} = \mathbf{u_s}/2$) to model the migration of the BASC away from the trench as new lithosphere is created and added to the arc plate. Finally, velocity along the internal boundary corresponding to the surface of the subducting plate from 0 to 70 km depth is prescribed so as to increase linearly with depth to a value equivalent to the subduction rate ($\mathbf{u} = \mathbf{u_c}$). This is done to account for partial decoupling of the slab and mantle at shallow depths within the mantle wedge, as inferred from a comparison of geodynamic models of subduction to observations of heat flow across arcs [*Wada and Wang*, 2009].

[12] Temperature along the top surface of the model domain (T_o) is held fixed at 0°C while temperature along the side boundaries of the model are fixed to a half-space cooling model plus adiabatic effects:

$$T(z,t) = \left((T_m - T_o)\mathrm{erf}\left(\frac{z}{2\sqrt{\frac{k}{\rho C_p} t}} \right) + T_o \right) + z\Delta T_{adb}, \quad (6)$$

where z is depth, T_o and T_m are the potential temperature of the surface and of the mantle, ΔT_{adb} is the adiabatic gradient, and t is time, corresponding to either the age of the subducting plate (t_{sp}) or the age of the overriding plate (t_{op}). The bottom boundary of the model is insulating.

3. Results

[13] A series of numerical experiments modeling mantle flow, temperature and melting in an arc-BASC system was undertaken to characterize the thermal and compositional evolution of the sub-arc mantle as the result of spreading in the back-arc. Experiments model a period of 20 Myr in the evolution of the system, beginning 10 Myr prior to the start of spreading. This phase of the system's evolution was modeled to insure that any transient related to the initial conditions would be minimal by the time spreading commenced.

[14] Temperature and depletion within the mantle wedge at a fixed distance of 125 km from the trench are used to characterize changes in the sub-arc mantle with time in the experiments. The location of this nominal arc was chosen to coincide with the point at which the slab is 125 km below the surface, consistent with the global mean value of depth to the slab surface beneath arcs [*Syracuse and Abers*, 2006].

[15] The thermal and compositional evolution of the mantle wedge is presented for a reference experiment (experiment 1, Table 2). The characteristics of this experiment are broadly representative of all of the experiments. Subsequently, the effects of subduction rate (u_c), spreading rate (u_s), mantle potential temperature (T_m), the age (which controls the thickness) of the overriding plate (t_{op}), and the initial location of spreading in the back-arc relative to the arc (Δx_o), are investigated through suites of experiments in which a single parameter is varied systematically. The range of values adopted for each parameter was chosen to be representative of that observed in subduction zones and back-arc systems globally [*Jarrard*, 1986; *Kelly et al.*, 2006;

Table 2. Description of the Numerical Experiments[a]

Experiment	Subduction Rate (km Myr^{-1})	Spreading Rate (km Myr^{-1})	Potential Temperature (°C)	Plate Age (Myr)	Arc - BASC Distance (km)
		Reference			
1	100	50	1350	50	25
		Subduction Rate (u_c)			
2	50	50	1350	50	25
3	150	50	1350	50	25
4	200	50	1350	50	25
		Spreading Rate (u_s)			
5	100	25	1350	50	25
6	100	75	1350	50	25
7	100	100	1350	50	25
		Potential Temperature (T_m)			
8	100	50	1300	50	25
9	100	50	1400	50	25
10	100	50	1450	50	25
		Age, Overriding Plate (t_{op})			
11	100	50	1350	25	25
12	100	50	1350	75	25
		Initial Distance, Arc-BASC (Δx_o)			
13	100	50	1350	50	10
14	100	50	1350	50	50
15	100	50	1350	50	75

[a]Plate age refers to the age of the overriding oceanic plate at the onset of spreading in the back-arc.

Langmuir et al., 2006; *Syracuse and Abers*, 2006; *Wiens et al.*, 2006]. A complete account of the parameters employed in each of the fifteen experiments can be found in Table 2.

3.1. Thermal Evolution of the Sub-Arc Mantle

[16] Spreading in the back-arc results in growth of the arc plate as the BASC migrates away from the trench (Figure 2). Temperatures in the uppermost portion of the mantle wedge change markedly with the onset of spreading. This is seen in the evolution of temperature at fixed depths beneath the arc (Figure 3). After a period of adjustment from the initial conditions, temperatures beneath the arc decrease steadily as the lithosphere of the overriding plate cools with time, resulting in temperature profiles that resemble those of a half-space cooling model. When spreading starts, temperatures beneath the arc increase rapidly as warm mantle is drawn up from depth in response to the divergence of the surface plates. This results in thinning of both the thermal and rheological boundary layers associated with the overriding plate (Figure 4). This thinning is most pronounced at the location of the BASC itself, but the effect is evident along much of the upper boundary. The widespread distribution of thinning would likely be reduced with a more sophisticated treatment of the rheology of the overriding plate, in particular one including some form of brittle deformation to allow for localization of strain [*Behn et al.*, 2002; *Lin et al.*, 2010].

[17] As the BASC migrates away, temperatures beneath the arc plate again decrease steadily and the boundary layer thickens with time. This cooling is slightly accelerated at intermediate depths as mantle that has experienced melting, and consequently the removal of latent heat, beneath the BASC is advected beneath the arc. This additional, localized cooling effect is evident at depths of 50–60 km during the period between 2 and 4 Myr after the onset of spreading in Figure 4.

3.2. The Evolution of Mantle Flow

[18] The changing position of the BASC relative to the trench leads to a strong time-dependence in mantle flow at arc-BASC systems. The complex flow patterns that result can be visualized using streamlines, which lie tangent to the velocity field at any instant in time (Figure 5a). In a velocity field that changes with time, streamlines also change with time. Prior to the onset of spreading, mantle is drawn in toward the corner of the wedge and down along the surface of the subducting plate. During this period, streamlines remain essentially constant with time, with the exception of

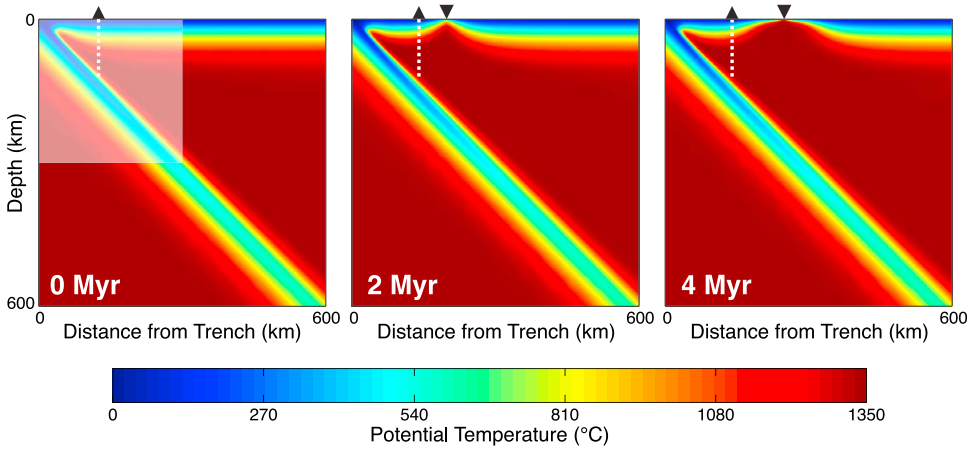

Figure 2. Potential temperature at three different times after the onset of spreading at the BASC for the reference experiment (experiment 1). The nominal location of the arc is indicated by a small, black triangle with a vertical dotted line extending beneath to indicate the location of sub-arc profiles shown in subsequent figures. The shaded region corresponds to the portion of the model domain shown in Figures 5 and 7.

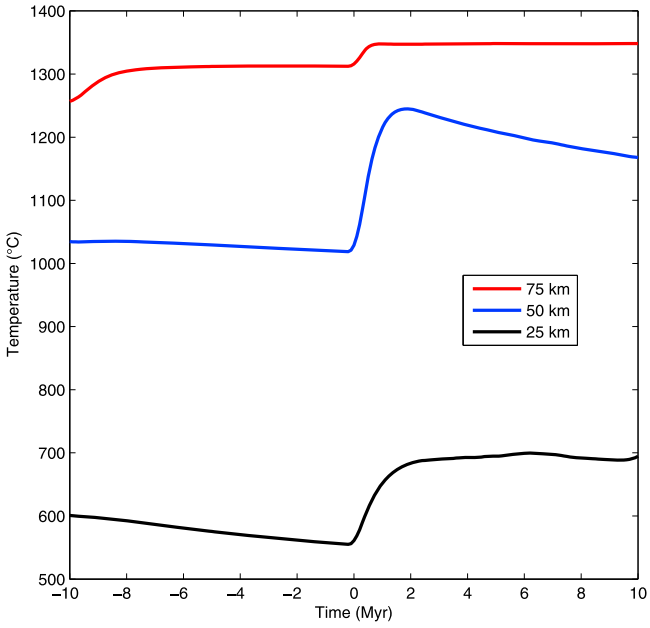

Figure 3. The evolution of temperature at three different depths beneath the nominal arc for the reference experiment (experiment 1). Time is given relative to the onset of spreading at the back-arc, with negative values indicating time prior to the onset of spreading at the BASC.

minor changes associated with the gradual thickening of the cold, viscous boundary layer beneath the overriding plate. Once spreading commences, this simple corner flow is modified. Streamlines become much steeper and diverge beneath the BASC as some mantle is drawn in toward the corner of the wedge by slab-induced flow while the rest is dragged away by the motion of the back-arc plate. This general flow pattern persists as the system continues to evolve, with the location of upwelling changing as the BASC moves away from the trench.

3.3. Melting and the Compositional Evolution of the Sub-Arc Mantle

[19] Melting is modeled using the Lagrangian particle method of *Hall and Kincaid* [2003], modified to use the hydrous peridotite melting parameterization of *Katz et al.* [2003]. In particular, the degree to which an individual parcel of mantle (i.e., particle) melts at a given time is calculated based upon its temperature, pressure, water content and history of melting and melt extraction (i.e., depletion) up to that time. Because flow in arc-BASC systems is time-dependent, the actual trajectories taken by individual particles (i.e., pathlines) will differ from the streamlines that describe the velocity field (Figure 5b). As a result, individual particles can have complicated melting histories, and patterns of melting and depletion within the mantle wedge can be complex. The pressure-temperature paths of two representative particles, whose physical trajectories are shown in Figure 5b, are seen in Figure 6. While these two particles are located on the same side of the BASC and at the same depth at the time of the onset of melting, their physical and compositional evolutions are very different. Both particles experience decompression immediately following the onset of spreading, as they are drawn upwards by the divergent motion of the overriding plate, leading them to cross the dry peridotite solidus. However, the particle closest to the initial location of the BASC (particle A), which was drawn in toward the corner of the wedge, passes beneath the arc before being entrained in the cold boundary layer above the subducting slab and dragged downward by slab-induced flow. Consequently, this particle cools after reaching temperatures only slightly above the dry peridotite solidus. At the same time, the particle that started further from BASC (particle B) gets entrained by the migrating BASC, and experiences substantial decompression melting before being

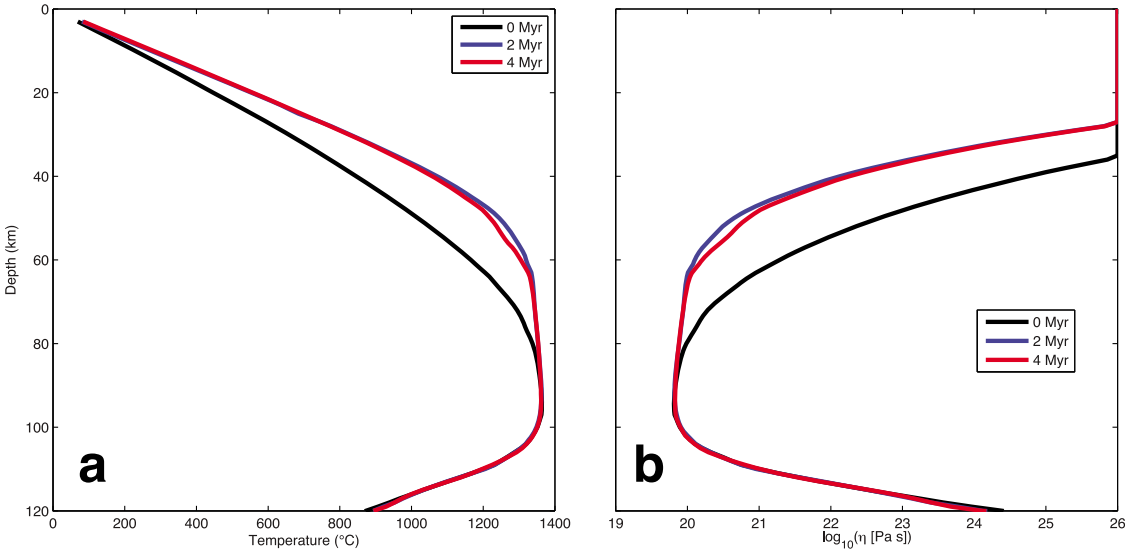

Figure 4. Profiles of (a) temperature and (b) viscosity directly beneath the nominal arc at three different times after the onset of spreading at the BASC for experiment 1. The upper 100 km of the 0 Myr temperature profile is identical to that of a half-space cooling profile for 50 Myr old lithosphere. The influence of the cold subducting plate is evident in the lowermost portion of the profiles.

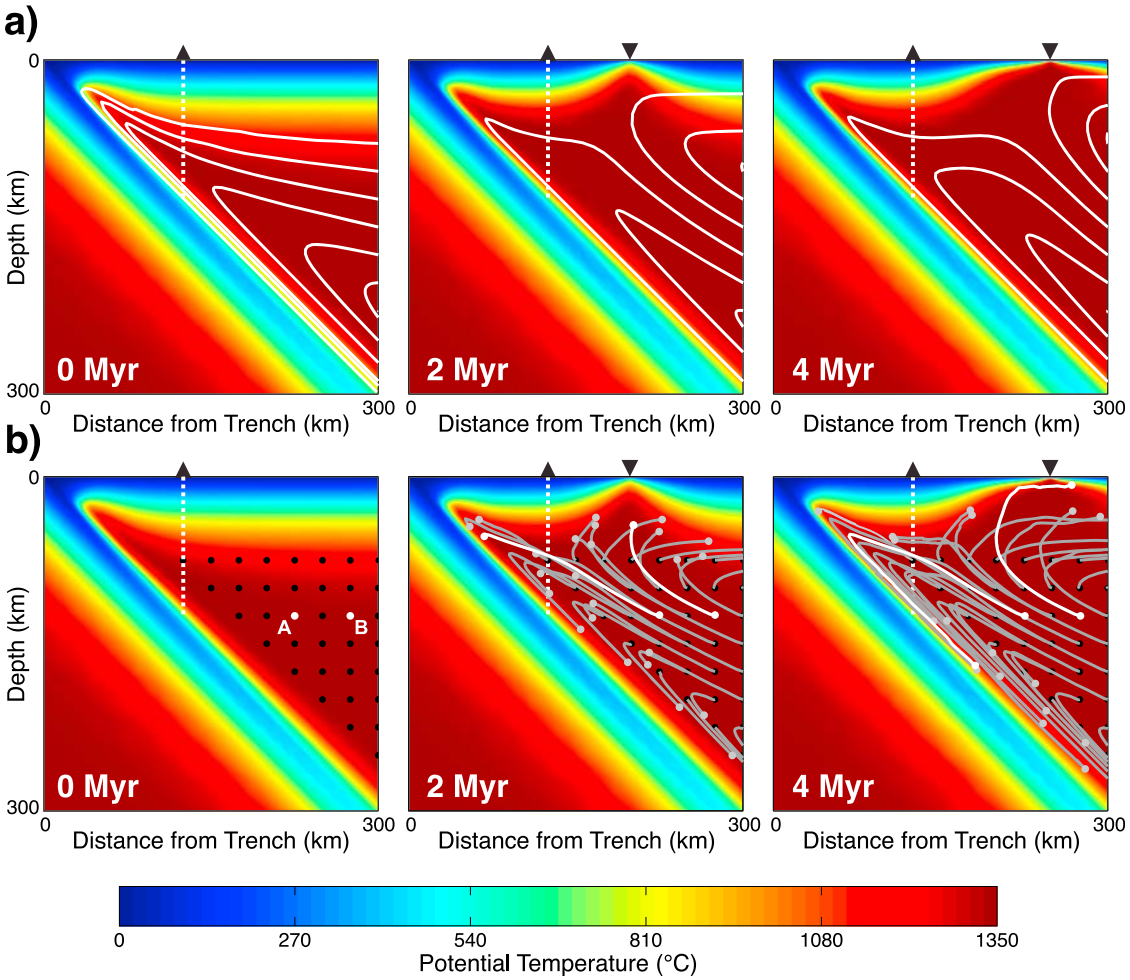

Figure 5. Flow within the mantle wedge at three different times following the onset of spreading at the BASC for experiment 1, illustrated using (a) instantaneous streamlines and (b) particle pathlines. Particle pathlines (gray lines with gray dots indicating current particle position) are shown for a set of 36 particles initially arranged in a regular grid (i.e., at t = 0 Myr), as shown by the black dots. The evolution of two of these particles, labeled A and B and shown in white, is highlighted in Figure 6.

incorporated into the lithosphere and cooling. These two classes of particle trajectories are characteristic of distinct regions within the mantle wedge [*Lin et al.*, 2010].

[20] Prior to the onset of spreading at the BASC, active decompression melting is limited to a layer at the base of the lithosphere that extends into the corner of the mantle wedge (Figure 7a). The extent of melting in this layer is small and results in a thin layer of slightly depleted mantle above the surface of the subducting plate as the depleted residual is dragged downward by the motion of the slab. Once spreading begins at the BASC, the region of active melting expands in response to increasing temperatures as the cold thermal boundary layer is thinned, and a broad zone of melting develops beneath the BASC as a result of upwelling in the mantle.

[21] Melting beneath the BASC results in much more extensive depletion of the mantle, and depleted residual mantle generated by melting beneath the BASC is subsequently drawn beneath the arc. This results in a thicker, more highly depleted layer of residual mantle immediately above the surface of the subducting plate (Figure 7a). Beneath the arc, two regions of depleted mantle are evident (Figure 8). Prior to spreading at the BASC, a thin (~20 km) layer of depleted mantle is found immediately above the slab while a second, slightly less depleted layer is found at the base of the lithosphere. After spreading begins at the BASC, each of these layers becomes steadily more depleted with time as material that rose to progressively shallower depths beneath the BASC is gradually entrained by the slab-driven flow and drawn beneath the arc. The lower layer is consistently slightly more depleted than the upper layer, as a result of the small amount of decompression melting that occurs in the shallowest portion of the mantle wedge, near the corner.

[22] To evaluate potential effects related to the choice of water content, the experiment was repeated assuming a perfectly dry mantle source (Figure 7b). An anhydrous mantle results in a greatly reduced region of active melt generation, relative to the reference experiment. In addition, the maximum extent of depletion is slightly lower for the anhydrous case. However, overall the spatial and temporal pattern of melt generation and depletion does not differ significantly from the reference experiment.

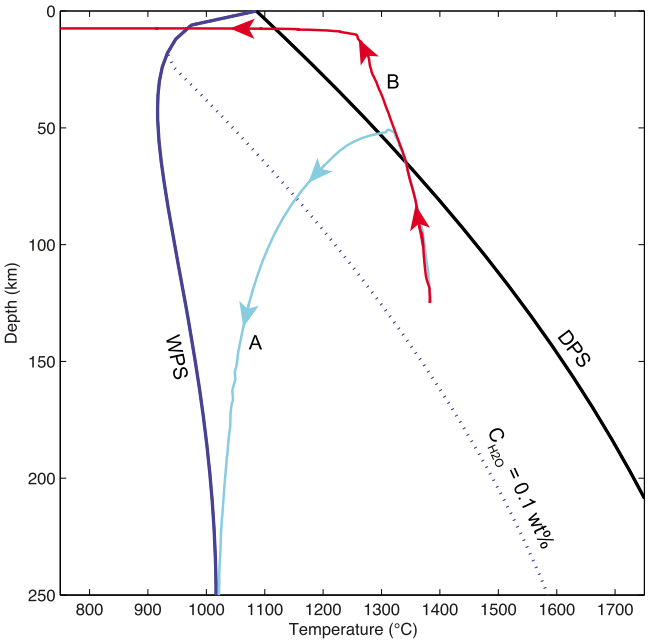

Figure 6. Evolution of two representative groups of particles within the mantle wedge, as demonstrated by the particles shown as A and B in Figure 5b, in pressure (depth)-temperature space. The solidii for dry peridotite (DPS), water saturated peridotite (WPS), and peridotite with a bulk water content of 0.1 wt% of *Katz et al.* [2003] are shown for reference.

3.4. Effects of Kinematic Parameters and Initial Thermal Structure

[23] To more fully characterize the evolution of the sub-arc mantle in arc-BASC systems, numerical experiments were undertaken to consider the effect of various kinematic factors, including subduction rate (u_c), back-arc spreading rate (u_s), and the initial location of spreading in the back-arc relative to the arc (Δx_o). Experiments were also conducted to evaluate the influence of the initial thermal structure of the mantle, in the form of mantle potential temperature (T_m) and the age of the overriding plate (t_{op}), on the evolution of the sub-arc mantle. Experiments considered a range of values of each of these parameters so as to encompass the range observed at subduction zones and BASCs globally [*Jarrard*, 1986; *Kelly et al.*, 2006; *Langmuir et al.*, 2006; *Syracuse and Abers*, 2006; *Wiens et al.*, 2006]. A complete account of the particular parameter values for each of the experiments is given in Table 2.

[24] A series of four numerical experiments (1–4; Table 2) were conducted in which subduction rate (u_c) was varied systematically to characterize its effect on the system. Subduction rates of 50, 100, 150 and 200 km/Myr were evaluated. The initial appearance of depleted material in the shallow mantle beneath the arc is independent of subduction rate, as depletion increases at the same rate for all experiments during the 2 Myr period following the onset of spreading (Figure 9a). Following this initial period of rapid increase, depletion in the sub-arc mantle plateaus briefly before proceeding to increase steadily again, albeit at a lower rate. During this later phase, the rate at which depletion increased was found to vary with subduction rate, ranging from ~0.4 %/Myr at a subduction rate of 50 km/Myr to ~0.9 %/Myr at a subduction rate of 200 km/Myr. This difference reflects the fact that faster subduction rates lead to faster flow in the mantle and consequently more rapid advection of depleted mantle from beneath the BASC to the sub-arc region. The net result is that faster subduction rates lead to a more highly depleted sub-arc mantle than do slow subduction rates at any given time during this phase of the system's evolution.

[25] As with subduction rate, a suite of four numerical experiments (1, 5–7; Table 2) was conducted to evaluate the effect of the rate of spreading at the BASC (u_s) on the evolution of the sub-arc mantle. Depletion beneath the arc increases most rapidly during the period immediately following the initiation of spreading in the back-arc (Figure 9b). The rate of increase during this initial phase is a function of the spreading rate, with faster spreading rates leading to a more rapid increase in depletion of the sub-arc mantle, with rates varying from ~4 %/Myr at a spreading rate of 100 km/Myr to ~1.2 %/Myr at a spreading rate of 25 km/Myr. This difference is the result of faster spreading rates generating faster upwelling in the underlying mantle, resulting in a more rapid depletion within the mantle. Following this initial period, depletion within the mantle beneath the nominal arc plateaus for a period of ~1 Myr before continuing to increase at a lower rate. During this final phase, the rate of increase is essentially independent of spreading rate, at ~0.7 %/Myr. This reflects the fact that during this phase the increase in depletion is dominated by advection of depleted mantle from beneath the BASC to the arc, a process controlled by the subduction rate, which is held constant in this set of experiments. Overall, faster spreading rates lead to a greater maximum extent of depletion in the sub-arc mantle at any given time, mostly as the result of differences during the period immediately following the onset of spreading.

[26] The effect of the position of the BASC relative to the arc was investigated in a series of four experiments (1, 13–15; Table 2) in which the initial distance between the BASC and the arc (Δx_o) was varied from 10 km to 75 km. Immediately following the onset of spreading in the back-arc, depletion of the sub-arc mantle increases rapidly (Figure 9c). The maximum extent of depletion achieved during this phase varies with distance between the arc and the BASC, with the greatest depletion achieved for the shortest separations. Following this initial stage, depletion of the sub-arc mantle remains relatively constant for a period, the duration of which is related to the separation distance (shorter distances lead to shorter durations of this plateau). Subsequently, depletion again increases, at a rate (~0.6%/Myr) that is independent of arc-BASC separation distance. In general, at any given time after the onset of spreading in the back-arc, shorter initial separation distances lead to greater depletion.

[27] Four experiments (1, 8–10; Table 2) were conducted in which mantle potential temperature (T_m) was varied between 1300 °C and 1450 °C. Differences in mantle potential were found to lead to differences in the depletion of the sub-arc mantle prior to the start of spreading, with higher temperatures allowing greater extents of melting and depletion beneath the arc (Figure 9d). With the onset of spreading, depletion of the sub-arc mantle initially increases rapidly

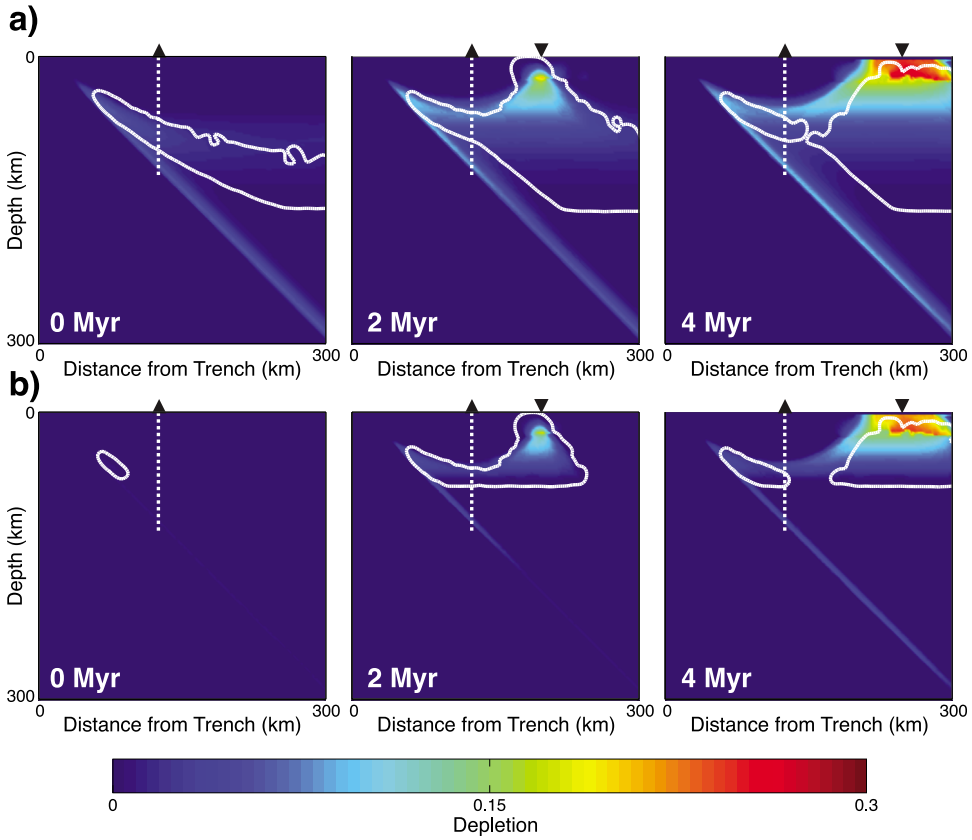

Figure 7. Evolution of melting and depletion within the mantle following the onset of spreading at the BASC for experiment 1 assuming a uniform water content of (a) 0.1 wt% and (b) 0 wt% in the mantle wedge. Areas in which melt is actively being generated are outlined in white while the depletion of the mantle (i.e., accumulated extent of melting and melt extraction experienced by the mantle up to that time) is shown by the background color.

before leveling off for a period of ~1 Myr. During this phase, the rate at which depletion increases is slightly greater for higher mantle potential temperatures, ranging from ~1.5–3%/Myr. Subsequently, the rate of depletion increases more gradually, at a rate (~0.6%/Myr) that is largely independent of temperature.

[28] The presence of an overriding plate limits the depths to which mantle can ascend. Consequently, the thickness of this plate can influence the extent of decompression melting experienced by upwelling mantle. A set of three experiments (1, 11–12; Table 2) was undertaken to evaluate the effect of the thickness of the overriding plate on melting in arc-BASC systems. As the overriding plate was assumed to be oceanic lithosphere, its initial temperature was defined using a half-space cooling model (6), allowing the thickness of the lithosphere to be controlled by varying its age (t_{op}). The initial age of the overriding plate was varied between 15 Myr and 65 Myr in these experiments, resulting in plate ages at the start of spreading at the BASC ranging from 25 Myr to 75 Myr.

[29] The thickness (age) of the overriding plate was found to determine the depletion of the sub-arc mantle before the onset of spreading in the back-arc, with thinner (younger) plates allowing for melting at shallower depths and greater extents of depletion (Figure 9e). With the onset of spreading, depletion of the sub-arc mantle increases rapidly, at a rate

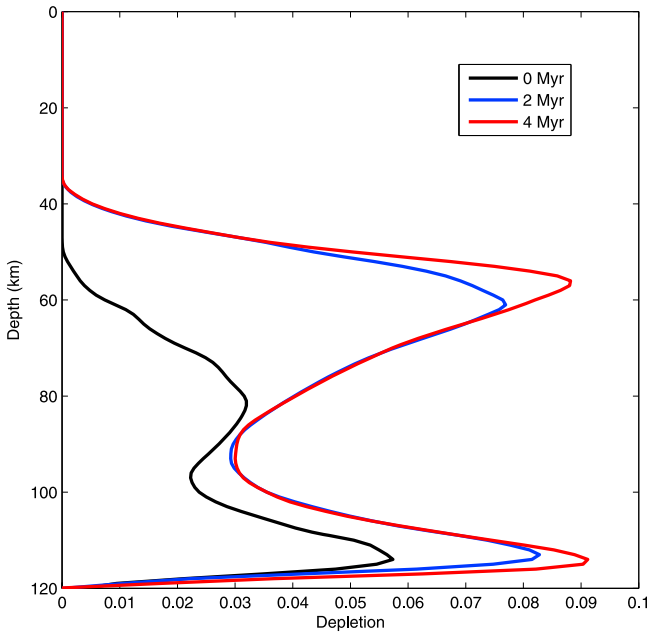

Figure 8. Depletion of the mantle wedge beneath the arc following the onset of spreading at the BASC for the reference experiment (experiment 1).

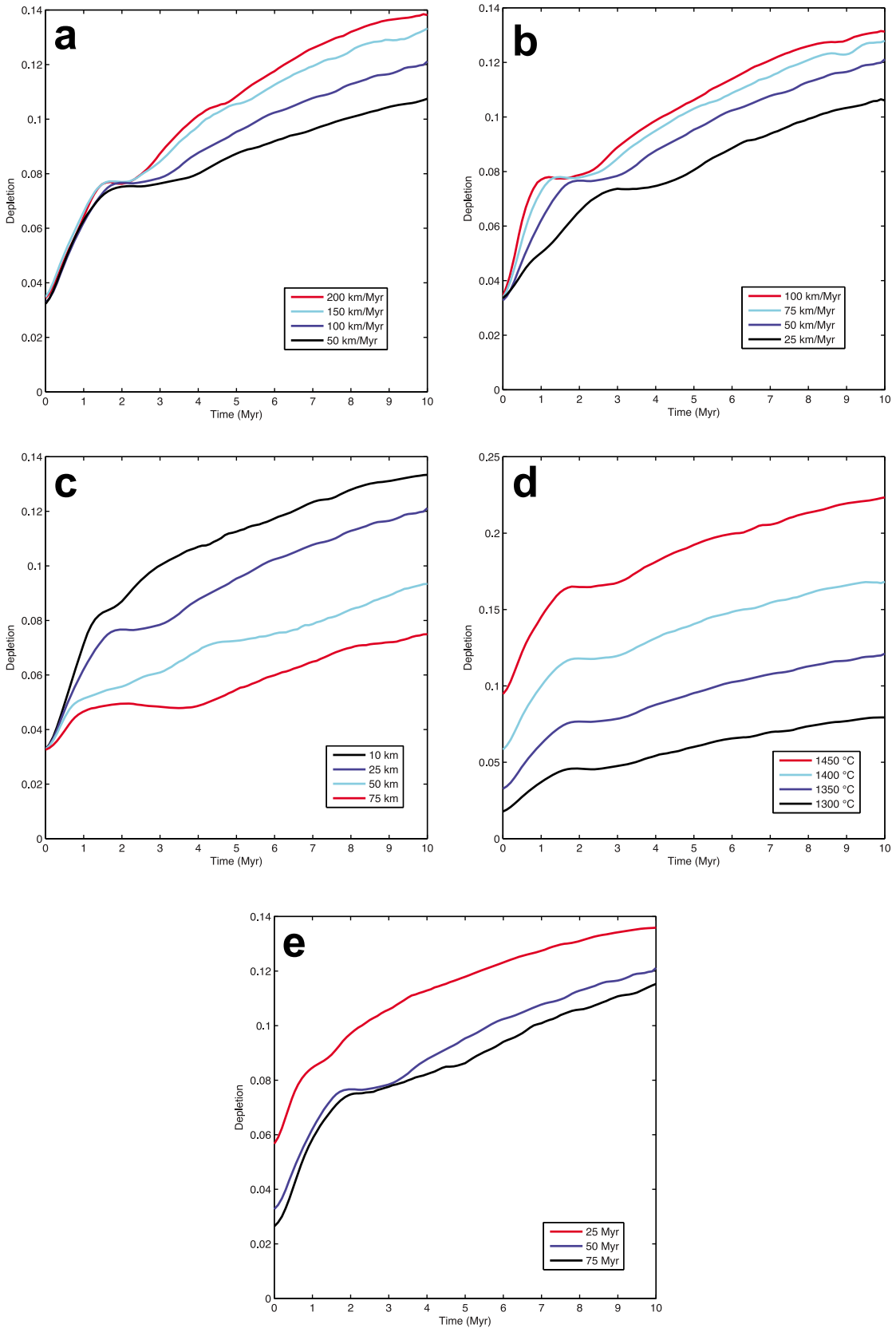
a
Depletion
Time (Myr)
200 km/Myr
150 km/Myr
100 km/Myr
50 km/Myr
b
Depletion
Time (Myr)
100 km/Myr
75 km/Myr
50 km/Myr
25 km/Myr
c
Depletion
Time (Myr)
10 km
25 km
50 km
75 km
d
Depletion
Time (Myr)
1450 °C
1400 °C
1350 °C
1300 °C
e
Depletion
Time (Myr)
25 Myr
50 Myr
75 Myr

Figure 9

(~2%/Myr) independent of plate thickness. Subsequently, depletion of the sub-arc mantle levels off before again increasing steadily at a reduced rate (~0.5%/Myr) that is again, largely independent of plate thickness. Overall, at any given time after spreading commences, thinner (younger) overriding plates lead to a greater extent of depletion.

4. Discussion

[30] These results suggest that spreading at the BASC significantly alters flow, temperature, and composition in the mantle beneath the adjacent arc. Furthermore, the sub-arc mantle is shown to experience substantial changes over time as a result of spreading in the back-arc. This change can be separated into two phases. There is an initial period of rapid change over the first 2 Myr following the onset of spreading during which temperatures in the sub-arc mantle increase markedly and maximum depletion in the sub-arc mantle increases by ~4% in almost all experimental scenarios. This is followed by a period of more gradual change, in which temperatures slowly decrease while depletion increases. These two stages reflect two distinct mechanisms at work in the sub-arc mantle. During the initial stage, depletion increases as a result of enhanced upwelling throughout the sub-arc mantle and a concurrent increase in mantle temperature directly beneath the arc, as warm mantle is first drawn upwards from depth in response to extension in the back-arc. That is to say, the increase in depletion beneath the arc is largely generated *in situ* by enhanced melting beneath the arc, and the rate of increase is largely controlled by the spreading rate at the BASC, with faster spreading leading to a more rapid depletion of the mantle. Once the new flow pattern and thermal state is established, the maximum extent of depletion beneath the arc reaches a plateau at a new constant value (~8% for a mantle temperature of T_m = 1350°C and an overriding plate age of t_{op} = 50 Myr or more). During the second stage, mantle that has been depleted by melting at increasingly shallower depths beneath the BASC is advected beneath the arc by slab-induced corner flow, resulting in a gradual increase in depletion beneath the arc. The rate at which depletion increases during this phase is largely controlled by the subduction rate, with faster subduction leading to more rapid advection of depleted material beneath the arc from the BASC.

[31] The increase in temperatures within the shallow sub-arc mantle (Figure 3) and the simultaneous thinning of the lithosphere beneath the arc (Figure 4) predicted by the numerical experiments should result in geochemically observable consequences. For example, one would expect to see an increase in the extent of melting in the mantle beneath the arc following the onset of spreading at the BASC, as a result of the increased mantle temperature. The eruption of boninitic magmas in the fore-arc in the West Philippine – Mariana region coincident with the onset of spreading [*Crawford et al.*, 1981] may be one example of this effect. One might also expect a shallowing in the depth of equilibration for arc magmas as a result of thinning of the arc. This effect might manifest itself as variations in the influence of garnet on the melt, which could cause variations in the fractionation of heavy and middle rare earth elements. This is seen along the East Philippine Arc, where the arc lithosphere is in the process of thinning in response to the recent southward propagation of subduction [*Macpherson*, 2008].

5. Depletion Beneath the Tonga Arc

[32] The Tonga arc and the BASCs of the adjacent Lau basin provide an opportunity to test the trends observed in the numerical experiments. The formation of the Lau Basin by the southward propagation of spreading in the back-arc, in response to trench retreat and slab rollback [*Hall*, 2002], creates a unique setting in which the temporal evolution of an arc-BASC system perpendicular to strike can, to some degree, be mapped to location along strike. The analogy is imperfect, as there are systematic variations in subduction and spreading rates from north to south, with the fastest rates in the north [*Bevis et al.*, 1995; *Zellmer and Taylor*, 2001]. Furthermore, slab rollback introduces a toroidal component to mantle flow around the subducting plate, and would be expected to result in southward-directed along-strike flow in the mantle beneath Tonga [*Kincaid and Griffiths*, 2003; *Schellart et al.*, 2007], a prediction that is consistent with observations of trench parallel seismic anisotropy beneath Tonga [*Smith et al.*, 2001] and north-south variations in the isotopic composition of magmas [*Pearce et al.*, 2007]. However, the portion of the Tonga Arc adjacent to the Eastern Lau Spreading Center (ELSC) and the Valu Fa Ridge (VFR) (i.e., 20 °S – 23 °S) is relatively continuous and has a simple geometry (Figure 10), making it an appropriate point of comparison for the numerical model. In particular, the linearity of both the arc and the BASC in this region, combined with its relative isolation from the edges of the slab, helps to minimize the significance of any 3-dimensional mantle flow, which could not be resolved by our 2-dimensional model.

[33] We use samples from three submarine (Volcanoes A, 1 and 7) and one subaerial (Ata) volcano from this portion of the arc to characterize variations in the extent to which the sub-arc mantle is depleted prior to melting beneath the arc. These volcanoes span a range of arc-BASC separation distances, from 34 km at Volcano 7, in the south, to 70 km to the north at Volcano A. We calculate the extent of prior depletion due to melting beneath the BASC using a two-step batch melting approach to reproduce observed variations in Ti_6 in the arc magmas [*Cooper et al.*, 2010]. Conceptually, we begin with a fertile mantle source in the back-arc, which experiences an initial phase of decompression melting beneath the BASC, generating a depleted residuum. This residuum is then advected beneath the arc where it experiences a second phase of melting via flux melting to produce a melt that is erupted at the arc along with a highly depleted residuum. We assume the fertile

Figure 9. Maximum extent of depletion beneath the nominal arc following the onset of spreading at the BASC for numerical experiments with different (a) subduction rates, u_c (experiments 1–4); (b) back-arc spreading rates, u_s (experiments 1 and 5–7); (c) distances between the nominal arc and the initial location of spreading in the back-arc, Δx_o (experiments 1 and 13–15); (d) mantle potential temperatures, T_m (experiments 1 and 8–10); and (e) ages for the overriding lithosphere, t_{op} (experiments 1 and 11–12). A complete description of the individual experiments is given in Table 2.

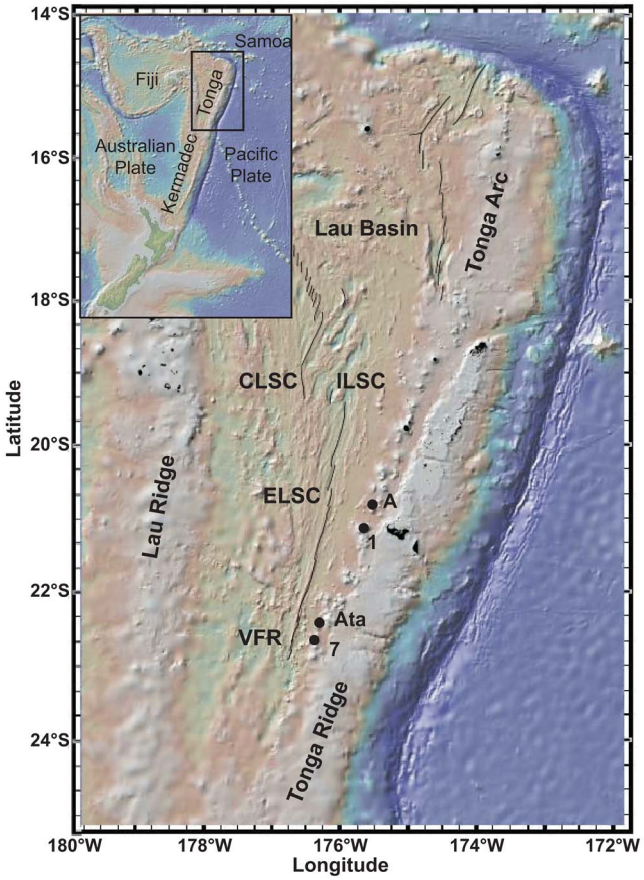

Figure 10. Bathymetric map of the southwest Pacific in the vicinity of Tonga. Small black circles show the location of the three submarine (A, 1 and 7) and one subaerial (Ata) volcanoes discussed in the text. A number of BASCs in the region, including the Central Lau Spreading Center (CLSC), Intermediate Lau Spreading Center (ILSC), Eastern Lau Spreading Center (ELSC) and the Valu Fa Ridge (VFR) are labeled.

mantle starts with 0.133 wt% TiO_2 and a bulk partition coefficient for TiO_2 of 0.04, as in the work of *Kelley et al.* [2006]. We then solve for the depletion associated with the first phase of melting beneath the BASC necessary to produce the values of Ti_6 observed at each of the arc volcanoes. For any single value of the extent of melting beneath the arc, there is a strong positive correlation between the extent of depletion and the arc-BASC distance, as predicted by the numerical experiments. In particular, the data show a clear trend of increasing sub-arc depletion from south (Volcano 7) to north (Volcano A), which is equivalent to increasing depletion over time at a fixed location along the arc, and consistent with the observations of *Cooper et al.* [2010]. In Figure 11, values of depletion due to melting beneath the BASC are plotted as a function of distance from the BASC for each of the four volcanoes assuming 5% melting occurs beneath the arc. This choice for the extent of melting is likely too low as a result of the simplicity of some of our assumptions (i.e., batch melting, uniformly depleted source). Nonetheless, the calculation is illustrative of the rapid increase in depletion of the sub-arc mantle with increasing arc-BASC separation, as predicted by the numerical experiments. Predicted average depletion of the sub-arc mantle over depths of 40–80 km from experiments 1 and 8–10 is plotted in Figure 11 for comparison with the observations. While the experimental results do not match the slope of the trend in the observations in detail, the pattern of increasing depletion with increasing arc–BASC separation in the predictions and the data are qualitatively similar, particularly for the experiments with mantle potential temperatures of 1400–1450°C. This is consistent with seismic and petrologic observations showing relatively high mantle temperatures beneath Tonga and the Lau Basin [*Wiens et al.*, 2006]. At least some of the mismatch between the predictions and the observations can be attributed to the generic character of the numerical experiments. In particular, we would expect experiments incorporating a slab geometry more appropriate to the region with more precisely matched tectonic forcing and overriding plate thickness to produce a better match to the observations than the present experiments. Such tailored experiments are the subject of ongoing work.

6. Conclusions

[34] We have presented results from a series of 2-D numerical experiments designed to characterize the thermal

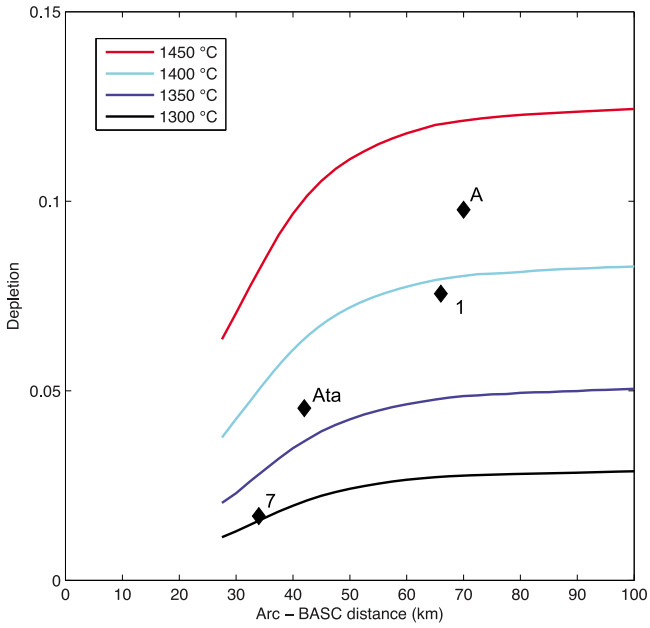

Figure 11. Observations and predictions of depletion beneath the arc due to melting at the BASC as a function of distance between the arc and the BASC. Observations are from three submarine volcanoes (A, 1 and 7) and one subaerial (Ata) volcano in the Tonga Arc, whose mantle sources are thought to be depleted by melting beneath the adjacent Eastern Lau Spreading Center and Valu Fa Ridge (see Figure 10). Depletion is determined using a two-step batch melting approach to reproduce variations in Ti_6 (TiO_2 concentration at 6 wt% MgO) in the Tonga Arc magmas [*Cooper et al.*, 2010]. Distance between the arc and the BASC was estimated from bathymetric maps of the region. Model predictions of average depletion beneath the arc over the depth range of 40–80 km are shown for experiments 1 and 8–10, in which mantle potential temperature is varied.

and compositional evolution of the sub-arc mantle in arc-BASC systems. We find large changes in both the temperature and the composition of the sub-arc mantle as the BASC migrates away from the arc. In particular, experimental results indicate that temperatures in the mantle beneath the arc increase with the onset of spreading at the BASC. This occurs as the result of warm mantle being drawn upwards from depth in response to extension in the back-arc, effectively thinning the cold boundary layer beneath the overriding plate.

[35] Compositionally, the sub-arc mantle becomes increasingly more depleted with time following the onset of spreading, as mantle that has experienced decompression melting and melt extraction beneath the BASC is gradually drawn beneath the arc plate by corner flow induced by the motion of the subducting plate. The timing of the appearance of this depleted mantle beneath the arc is dictated by the proximity of the initial rifting to the arc, the rate of spreading in the back-arc, the thickness (age) of the arc plate, and the potential temperature of the mantle. The rate at which depletion increases in the sub-arc mantle is controlled by subduction rate. The predicted depletion is consistent with pre-conditioning models that explain the depletion of HFSEs relative to LILEs in arc magmas at arc-BASC systems by melting of the arc mantle source beneath the BASC prior to melting beneath the arc [*McCulloch and Gamble*, 1991; *Woodhead et al.*, 1993; *Caulfield et al.*, 2008]. The prediction of increasing depletion of the sub-arc mantle over time is consistent with observations of systematic along-strike variations in Ti_6 within the Tonga Arc as well as the two-stage melting model proposed by *Cooper et al.* [2010] to explain the occurrence of boninitic magmatism in the Tonga Arc as the result of flux melting of a highly depleted mantle source.

[36] **Acknowledgments.** L.B. Cooper and T. Plank were funded by NSF-OCE-0526450 and NSF-OCE-0839061 (to T. Plank). We thank two anonymous referees and the Associate Editor for their helpful reviews.

References

Behn, M. D., J. Lin, and M. T. Zuber (2002), A continuum mechanics model for normal faulting using a strain-rate softening rheology: implications for thermal and rheological controls on continental and oceanic rifting, *Earth Planet. Sci. Lett.*, *202*, 725–740.

Behn, M. D., G. Hirth, and P. B. Kelemen (2007), Trench-parallel anisotropy produced by foundering of arc lower crust, *Science*, *317*, 108–111.

Bevis, M., et al. (1995), Geodetic observations of very rapid convergence and back-arc extension at the Tonga arc, *Nature*, *374*, 249–251.

Cagniocle, A.-M., E. M. Parmentier, and L. T. Elkins-Tanton (2007), Effect of solid flow above a subducting slab on water distribution and melting at convergent plate boundaries, *J. Geophys. Res.*, *112*, B09402, doi:10.1029/2007JB004934.

Caulfield, J. T., S. P. Turner, A. Dosseto, N. J. Pearson, and C. Beier (2008), Source depletion and extent of melting in the Tongan sub-arc mantle, *Earth Planet. Sci. Lett.*, *273*, 279–288.

Conder, J. A. (2005), A case for hot slab surface temperatures in numerical viscous flow models of subduction zones with an improved fault zone parameterization, *Phys. Earth Planet. Inter.*, *149*, 155–164.

Cooper, L. B., T. Plank, R. J. Arculus, E. H. Hauri, P. S. Hall, and S. W. Parman (2010), High-Ca boninites from the active Tonga Arc, *J. Geophys. Res.*, *115*, B10206, doi:10.1029/2009JB006367.

Crawford, A. J., L. Beccaluva, and G. Serri (1981), Tectono-magmatic evolution of the West Philippine-Mariana region and the origin of boninites, *Earth Planet. Sci. Lett.*, *54*, 346–356.

Currie, C. A., and R. D. Hyndman (2006), The thermal structure of subduction zone back arcs, *J. Geophys. Res.*, *111*, B08404, doi:10.1029/2005JB004024.

Currie, C. A., K. Wang, R. D. Hyndman, and J. He (2004), The thermal effects of steady-state slab-driven mantle flow above a subducting plate: The Cascadia subduction zone and backarc, *Earth Planet. Sci. Lett.*, *223*, 35–48.

Dunn, R. A., and F. Martinez (2011), Contrasting crustal production and rapid mantle transitions beneath back-arc ridges, *Nature*, *469*, 198–202.

Hall, R. (2002), Cenozoic geological and plate tectonic evolution of SE Asia and the SW Pacific: Computer-based reconstructions, models and animations, *J. Asian Earth Sci.*, *20*, 353–431.

Hall, P. S., and C. Kincaid (2001), Diapiric flow at subduction zones: A recipe for rapid transport, *Science*, *292*, 2472–2475.

Hall, P. S., and C. Kincaid (2003), Melting, dehydration and the dynamics of off-axis plume-ridge interaction, *Geochem. Geophys. Geosyst.*, *4*(9), 8510, doi:10.1029/2003GC000567.

Harmon, N., and D. K. Blackman (2010), Effects of plate boundary geometry and kinematics on mantle melting beneath back-arc spreading centers along the Lau Basin, *Earth Planet. Sci. Lett.*, *298*, 334–346.

Hebert, L. B., P. Antoshechkina, P. Asimow, and M. Gurnis (2009), Emergence of a low-viscosity channel in subduction zones through the coupling of mantle flow and thermodynamics, *Earth Planet. Sci. Lett.*, *278*, 243–256.

Hirschmann, M. M., T. Tenner, C. Aubaud, and A. C. Withers (2009), Dehydration melting of nominally anhydrous mantle: The primacy of partitioning, *Phys. Earth Planet Inter.*, *176*, 54–68.

Honda, S., and M. Saito (2003), Small-scale convection under the back-arc occurring in the low viscosity wedge, *Earth Planet. Sci. Lett.*, *216*, 703–715.

Jadamec, M. A., and M. I. Billen (2010), Reconciling surface plate motions with rapid three-dimensional mantle flow around a slab edge, *Nature*, *465*, 338–341.

Jarrard, R. D. (1986), Relations among subduction parameters, *Rev. Geophys.*, *24*, 217–284.

Katz, R. F., M. Spiegelman, and C. H. Langmuir (2003), A new parameterization of hydrous mantle melting, *Geochem. Geophys. Geosyst.*, *4*(9), 1073, doi:10.1029/2002GC000433.

Kelley, K. A., T. Plank, T. L. Grove, E. M. Stolper, S. Newman, and E. Hauri (2006), Mantle melting as a function of water content beneath back-arc basins, *J. Geophys. Res.*, *111*, B09208, doi:10.1029/2005JB003732.

Kelley, K. A., T. Plank, S. Newman, E. M. Stolper, T. L. Grove, S. Parman, and E. Hauri (2010), Mantle melting as a function of water content beneath the Mariana Arc, *J. Petrol.*, *51*(8), 1711–1738.

Kincaid, C., and R. W. Griffiths (2003), Laboratory models of the thermal evolution of the mantle during rollback subduction, *Nature*, *425*, 58–62.

Kincaid, C., and P. S. Hall (2003), Role of back arc spreading in circulation and melting at subduction zones, *J. Geophys. Res.*, *108*(B5), 2240, doi:10.1029/2001JB001174.

Langmuir, C. H., A. Bezos, S. Escrig, and S. W. Parman (2006), Chemical systematics and hydrous melting of the mantle in back-arc basins, in *Back-Arc Spreading Systems: Geological, Biological, Chemical and Physical Interactions*, *Geophys. Monogr. Ser.*, vol. 166, edited by D. M. Christie et al., pp. 87–146, AGU, Washington, D. C.

Lin, S.-C., B.-Y. Kuo, and S.-L. Chung (2010), Thermomechanical models for the dynamics and melting processes in the Mariana subduction system, *J. Geophys. Res.*, *115*, B12403, doi:10.1029/2010JB007658.

Macpherson, C. G. (2008), Lithosphere erosion and crustal growth in subduction zones: Insights from initiation of the nascent East Philippine Arc, *Geology*, *36*, 311–314.

Martinez, F., and B. Taylor (2002), Mantle wedge control on back-arc crustal accretion, *Nature*, *416*, 417–420.

McCulloch, M. T., and J. A. Gamble (1991), Geochemical and geodynamical constraints on subduction zone magmatism, *Earth Planet. Sci. Lett.*, *102*, 358–374.

Pearce, J. A., P. D. Kempton, and J. B. Gill (2007), Hf-Nd evidence for the origin and distribution of mantle domains in the SW Pacific, *Earth Planet. Sci. Lett.*, *260*, 98–114.

Ribe, N. M. (1989), Mantle flow induced by back-arc spreading, *Geophys. J. Int.*, *98*, 85–91.

Schellart, W. P. (2004), Kinematics of subduction and subduction-induced flow in the upper mantle, *J. Geophys. Res.*, *109*, B07401, doi:10.1029/2004JB002970.

Schellart, W. P. (2008), Kinematics and flow patterns in the deep mantle and upper mantle subduction models: Influence of the mantle depth and slab to mantle viscosity ratio, *Geochem. Geophys. Geosyst.*, *9*, Q03014, doi:10.1029/2007GC001656.

Schellart, W. P., J. Freeman, D. R. Stegman, L. Moresi, and D. May (2007), Evolution and diversity of subduction zones controlled by slab width, *Nature*, *446*, 308–311.

Smith, G. P., D. A. Wiens, K. M. Fischer, L. M. Dorman, S. C. Webb, and J. A. Hildebrand (2001), A complex pattern of mantle flow in the Lau backarc, *Science*, *292*, 713–716.

Syracuse, E. M., and G. A. Abers (2006), Global compilation of variations in slab depth beneath arc volcanoes and implications, *Geochem. Geophys. Geosyst.*, *7*, Q05017, doi:10.1029/2005GC001045.

Syracuse, E. M., P. E. Van Keken, and G. A. Abers (2010), The global range of subduction zone thermal models, *Phys. Earth Planet. Inter.*, *183*, 73–90.

Taylor, B., and F. Martinez (2003), Back-arc basin basalt systematics, *Earth Planet. Sci. Lett.*, *210*, 481–497.

Toksoz, M. N., and A. T. Hsui (1978), Numerical studies of back-arc convection and the formation of marginal basins, *Tectonophysics*, *50*, 177–196.

van Keken, P. E., et al. (2008), A community benchmark for subduction zone modeling, *Phys. Earth Planet. Inter.*, *171*, 187–197.

Wada, I., and K. Wang (2009), Common depth of slab-mantle decoupling: Reconciling diversity and uniformity of subduction zones, *Geochem. Geophys. Geosyst.*, *10*, Q10009, doi:10.1029/2009GC002570.

Wiens, D. A., K. A. Kelley, and T. Plank (2006), Mantle temperature varaitions beneath back-arc spreading centers inferred from seismology, petrology, and bathymetry, *Earth Planet. Sci. Lett.*, *248*, 30–42.

Woodhead, J., S. Eggins, and J. Gamble (1993), High field strength and transition element systematics in island arc and back-arc basin basalts: Evidence for multi-phase melt extraction and a depleted mantle wedge, *Earth Planet. Sci. Lett.*, *114*, 491–504.

Zellmer, K. E., and B. Taylor (2001), A three-plate kinematic model for Lau Basin opening, *Geochem. Geophys. Geosyst.*, *2*, 1020, doi:10.1029/2000GC000106.

L. B. Cooper, Department of Mineralogy, University of Geneva, Geneva CH-1205, Switzerland. (lauren.cooper@erdw.ethz.ch)

P. S. Hall, Department of Earth Sciences, Boston University, 675 Commonwealth Ave., Boston, MA 02215, USA. (phall@bu.edu)

T. Plank, Lamont-Doherty Earth Observatory, Earth Institute at Columbia University, Palisades, NY 10964, USA. (tplank@ldeo.columbia.edu)